CrossMark

Towards Immobilized Proton-Coupled Electron Transfer Agents for Electrochemical Carbon Capture from Air and Seawater

Fawaz Ali,[1,=] David Bilger,[2,=] Evan D. Patamia,[2] Trisha L. Andrew,[2,z] and David G. Kwabi[1,z]

[1]Department of Mechanical Engineering, University of Michigan, Ann Arbor, Michigan 48109, United States of America
[2]Department of Chemistry, University of Massachusetts Amherst, Amherst, Massachusetts 01003, United States of America

Electrochemical CO_2 separation has drawn attention as a promising strategy for using renewable energy to mitigate climate change. Redox-active compounds that undergo proton-coupled electron transfer (PCET) are an impetus for pH-swing-driven CO_2 capture at low energetic costs. However, multiple barriers hinder this technology from maturing, including sensitivity to oxygen and the slow kinetics of CO_2 capture. Here, we use vapor phase chemistry to construct a textile electrode comprising an immobilized PCET agent, poly(1-aminoanthraquinone) (PAAQ), and incorporate it into redox flow cells. This design contrasts with others that use dissolved PCET agents by confining proton-storage to the surface of an electrode kept separate from an aqueous, CO_2-capturing phase. This system facilitates carbon capture from gaseous sources (a 1% CO_2 feed and air), as well as seawater, with the latter at an energetic cost of 202 kJ/mol$_{CO2}$, and we find that quinone moieties embedded within the electrode are more stable to oxygen than dissolved counterparts. Simulations using a 1D reaction-transport model show that moderate energetic costs should be possible for air capture of CO_2 with higher loadings of polymer-bound PCET moieties. The remarkable stability of this system sets the stage for producing textile-based electrodes that facilitate pH-swing-driven carbon capture in practical situations.

Anthropogenic carbon dioxide (CO_2) emissions continue to accrue in the atmosphere and raise global surface temperatures, thereby altering 10,000+ yearlong climate patterns.[1] The Intergovernmental Panel on Climate Change (IPCC) has provided guidance to mitigate this problem and prevent global temperatures from rising 1.5 °C above pre-industrial levels.[2,3] To this end, every mitigation route the IPCC proposed incorporated some form of CO_2 removal, which has spurred interest in capturing and converting/ sequestering carbon from both centralized and decentralized sources,[4] such as flue gas,[3] air,[5] and ocean water.[6] Current CO_2 capture methods employed on the industrial scale include absorption, adsorption, membrane separation, and cryogenic capture;[7] yet these approaches rely on high thermal loads that position energy consumption between 240 kJ/mol$_{CO2}$ (for flue gas capture using amine-functionalized solid sorbents)[8] and 800 kJ/mol$_{CO2}$ (for direct air capture using caustic soda).[5] In contrast, the energy consumption of CO_2 capture methods using electrochemical processes can fall below 100 kJ/mol$_{CO2}$[7,9] and be drawn from renewables, such as solar and wind, making them ideal for capturing carbon from decentralized feeds.[9–11]

Reversible redox-active compounds are one impetus for electrochemically mediated carbon capture when dissolved in ionic liquids,[12] dilute[13] or salt-concentrated[14] aqueous electrolytes, organic electrolytes,[15,16] or when restricted to a surface.[17] In the examples listed, the nucleophilicity of the capture agent is electrochemically modulated to bind and release CO_2 upon reduction and oxidation, respectively. Redox-active nucleophiles can also bind protons, making carbon capture from seawater intractable. Substitutes for nucleophilic binding include redox-active molecules that undergo proton-coupled electron transfer (PCET).[18] These PCET agents can be dissolved in an aqueous electrolyte and electrochemically driven to exchange protons with their surrounding medium,[19] allowing the solution pH and carbonate equilibria to shift accordingly until CO_2 is captured as dissolved inorganic carbon (DIC).[20–23] DIC comprises all inorganic carbon species that can be present in aqueous media (i.e., CO_2, HCO_3^- and CO_3^{2-}).

A downside to redox-active molecules is their sensitivity to chemical oxidation by atmospheric or dissolved molecular oxygen (O_2).[24] Any side-reaction with O_2, however minuscule, will lead to a cumulative loss in electrical efficiency with extended redox cycling, thereby necessitating complementary strategies to address O_2 sensitivity. Surprisingly, only a few attempts have been made to mitigate side-reactions with O_2 in flow cells that employ PCET agents for CO_2 capture. One approach involves meticulously designing/selecting PCET agents that are less sensitive to oxidative degradation in their reduced form, such as the phenothiazine, Neutral Red.[25] Another method is to impose an electrochemical "rebalancing" step to recover any capacity lost from parasitic side-reactions,[26] but this step costs energy and becomes impractical if chemical oxidation by O_2 occurs on a much shorter timescale than CO_2 capture. We envision a separate, yet complementary approach to the latter and former, one where PCET agents are immobilized on an electrode surface and decoupled from the CO_2-gas contactor (aqueous electrolyte). Several advantages follow from this idea: (1) The electrolyte can limit diffusion of molecular oxygen to the surface of the electrode, thereby minimizing parasitic side-reactions. (2) Any byproducts formed through side-reactions are unable to accumulate in the electrolyte. (3) The PCET agent and electrolyte-CO_2 contactor can be optimized independently. (4) CO_2 can be recovered from liquid sources, such as brines and seawater, without altering the configuration of the flow cell. As far as we know, mitigating oxygen sensitivity via the third strategy remains undemonstrated with PCET agents.

Solution synthesis and processing can polymerize and/or immobilize anthraquinone-based compounds for electrochemical carbon capture via nucleophilic binding, including poly(anthraquinone),[14] poly (vinyl anthraquinone),[27] and 2-aminoanthraquinone functionalized core-inter-shell particles.[28] In each of these systems, carbon nanotubes were incorporated into the polymer dispersions to improve charge mobility before being cast onto numerous carbon-based substrates such as cloths, felts, and paper. An alternative method to immobilize redox-active species involves vapor phase synthesis, where a conjugated monomer and chemical oxidant are sublimed over a substrate and subsequently polymerize on the surface.[29,30] These methods produce uniform and conformal films of conjugated polymers over microtextured surfaces[31–33] with thicknesses spanning

=Equal contribution.
zE-mail: tandrew@umass.edu; dkwabi@umich.edu

nanometers to microns.[34,35] Further, radical cationic intermediates produced during polymerization can react with functional groups on the substrate surface and immobilize polymer chains by chemical grafting. These details suggest vapor phase synthesis is a promising route toward immobilizing redox-active compounds for electrochemical carbon capture, especially in systems that operate under continuous-flow.

Here, we fabricate a redox-active electrode constituted by poly(1-aminoanthraquinone) (PAAQ) immobilized with doped poly(3,4-ethylenedioxythiophene): chloride (PEDOT:Cl) for electrochemical carbon capture using pH swing. The electrode is constructed atop affordable and commercially available blended wool felt textiles using vapor phase synthesis and exhibits remarkable stability when cycled over 100 h (about 4 d) under continuous flow. The electrode reversibly captures and releases CO_2 from a ca. 1% (0.01 bar) CO_2 feed and ocean water at energetic costs of 197 kJ/mol$_{CO2}$ and 202 kJ/mol$_{CO2}$, respectively. Reduced quinone moieties in the electrode were stable against chemical oxidation by oxygen in ambient air. The electrode was therefore able to facilitate CO_2 capture from air (in the presence of O_2), at an energetic cost of 553 kJ/mol$_{CO2}$. We put forth a one-dimensional (1-D) continuum reaction-transport model to explain the above observations and assist the community with future investigations.

Experimental

Materials and reagents.—All materials were used as received without further purification unless otherwise noted. 97% 1-aminoanthraquinone (1-AAQ), 97% 3,4-ethylenedioxythiophene (EDOT), and 97% iron (III) chloride (FeCl$_3$) were purchased from Millipore Sigma. 99% potassium chloride (KCl), 98.5% potassium ferrocyanide (K$_4$Fe(CN)$_6$), 98.5% potassium ferricyanide (K$_3$Fe(CN)$_6$), and 98% anthraquinone-2,6-disulfonic acid were purchased from Fisher Scientific. Instant Ocean Sea Salt was purchased from Petco. Graphite felt electrodes (CE Tech GF020) were purchased from Fuel Cell Store and wool felt/rayon (35%/65%) blend textiles were purchased from Joannes Fabrics (Hadley, MA).

Vapor phase synthesis.—Glass substrates were cleaned using the following procedure prior to any depositions: (1) sonication in a detergent solution for 5 min, (2) rinsing with DI water followed by additional sonication in acetone for 5 min, (3) immersion into boiling isopropanol for 5 min (2×), and (4) treatment with UV-ozone for 30 min.

A custom-built, quartz hot-wall reactor end-capped with KF flanges was used to synthesize conjugated polymers from the vapor phase according to an *oxidative chemical vapor deposition* procedure.[36]

PAAQ was synthesized and deposited by loading 1-AAQ and FeCl$_3$ into their respective crucibles. The crucibles were positioned in-line with 3 inches between them. The substrates (PET, glass, and graphite felt) were loaded into the reactor and placed between the two crucibles and adjacent to the crucible containing 1-AAQ. The pressure in the reactor was pumped down using an Edwards direct-drive vacuum pump to a pressure between 100–200 mtorr. BriskHeat resistive heat tapes were wrapped around the reactor walls where the monomer, substrates, and oxidant were placed. J-Kem thermocouples were secured between the heating tapes and reactor walls to monitor the temperature while it was ramped and maintained using a J-Kem Model Apollo temperature controller. The regions containing 1-AAQ and the substrates were heated to 160 °C, while those containing FeCl$_3$ were heated to 195 °C. The monomer and substrates began heating 45 s before the oxidant to maximize the intersectional area between vapors of 1-AAQ and FeCl$_3$. The deposition time was 17 min and taken from when the monomer began heating to when the heating tapes were switched off. The as-deposited films of 1-AAQ oligomers were rinsed with methanol until the solvent ran clear and subsequently washed in a methanol bath for 20 min to extract unreacted byproducts.

Multilayer electrodes were fabricated using three sequential depositions.

Deposition 1 (PEDOT:Cl coating).—EDOT was placed in a glass ampule and coupled with a Swagelok needle valve. The valve was then coupled to a glass inlet on the hot-wall reactor. FeCl$_3$ was loaded into a ceramic crucible and positioned in the reactor ca. 3 inches from the monomer inlet. A 2 × 3-inch wool felt blend swatch was placed between the monomer inlet and oxidant crucible. The reactor was pumped down to between 100–200 mtorr and three separate resistive heating tapes were wrapped around the regions containing the monomer, oxidant, and substrate. The three regions were simultaneously heated to 97 °C, 115 °C, and 195 °C, corresponding to the monomer, substrate and oxidant, respectively. The needle-valve was opened 12 min after heating began to introduce EDOT vapor into the reactor. The deposition lasted a total of 31 min, taken from when the reagents began heating to when the heating was switched off. The as-deposited film of poly(3,4-ethylenedioxythiophene): chloride was rinsed with methanol until the solvent ran clear and subsequently washed in an 0.5 M aqueous HCl bath for 30 min to extract unreacted byproducts.

Deposition 2 (PAAQ coating).—A 5 cm^2 wool felt blend swatch coated with PEDOT:Cl was placed in the reactor 3 inches from a crucible loaded with FeCl$_3$. 1-AAQ monomer was placed atop the coated swatch to maximize loading over the course of the deposition. The pressure in the reactor was pumped down and maintained between 100–200 mtorr. Resistive heating tapes were wrapped around the reactor walls and used to heat FeCl$_3$ to 195 °C and the substrates and 1-AAQ to 160 °C. The monomer and substrates began heating 45 s before the oxidant to maximize the intersectional area between vapors of 1-AAQ and FeCl$_3$. The deposition time was 17 min and taken from when the monomer began heating to when the heating tapes were switched off. The as-deposited films were stored in a vacuum oven at ambient temperature until a PEDOT:Cl capping layer could be deposited.

Deposition 3 (PEDOT:Cl capping layer).—The wool felt blend textiles coated with PEDOT:Cl and PAAQ were loaded into the reactor according to the same reagent arrangements discussed in deposition 1. Further, the deposition was performed using the same parameters as deposition 1, except for the deposition time, which lasted 17 min as opposed to 31 min. The as-deposited multilayer electrodes were rinsed with methanol until the solvent ran clear and subsequently washed with methanol for 20 min to extract unreacted byproducts.

Chemical characterization of PAAQ and electrodes.—Acetone was used to extract soluble fractions of PAAQ from pre-washed films for chemical characterization. Absorption spectra were collected using an Agilent 8453 spectrophotometer. Acetone was used as a solvent for all samples measured in solution. Mass spectra were acquired using an ultrafleXtreme MALDI-TOF mass spectrometer (Bruker Instruments, Billerica MA). The instrument was equipped with a Smartbeam™ laser at 355 nm, and all samples were run without a matrix in reflectron mode. Attenuated total reflectance infrared spectra (AT-IR) was acquired on a Bruker Alpha-p spectrophotometer. For PAAQ, soluble aliquots dissolved in acetone were dropcast onto the ATR stage until enough material was present for data acquisition. Multiple measurements were taken as acetone evaporated from the sample until peaks corresponding to the solvent were undetectable save for one band at ca. 1718 cm^{-1}, attributable to a carbonyl stretch.

The surface morphologies of PAAQ thin films were measured on glass using an Asylum Jupiter XR atomic force microscope (AFM). Images were acquired under tapping mode with a PPP-NCHR cantilever (force constant = 42 N m^{-1}, Nanosensors, Switzerland).

Images and elemental maps of the electrodes were collected using a Magellan 400 field-emission scanning electron microscope

(SEM). Images were acquired using a 5 kV accelerating voltage, while elemental maps from energy-dispersive X-ray (EDX) spectroscopy were collected using 15 kV, unless otherwise noted. An exception was made for pristine wool felt blend textiles, which were acquired using a 1 kV accelerating voltage to reduce charging. Given that PEDOT:Cl capping layers diminish the X-ray signals from nitrogen, electrode samples for EDX measurements were prepared by simultaneously depositing PEDOT:Cl and PAAQ to produce blended films, allowing the nitrogen signal to be detected and mapped to confirm uniformity.

Flow cell cycling.—Flow cell experiments were constructed with cell hardware from Fuel Cell Technologies (Albuquerque, NM), assembled into a zero-gap configuration. Pyrosealed POCO graphite flow plates with interdigitated flow patterns were used for both electrodes. The electrode in the excess-capacity side of the cell comprised a 5 cm^2 geometric surface area covered by a single sheet of CE Tech GF020 graphite felt (Fuel Cell Store) pre-baked in air for 12 h at 400 °C. The capacity-limiting side of the cell contained the active electrode under investigation (e.g., PAAQ) and was separated from the excess-capacity electrolyte by a Fumasep FKS-50 cation-exchange membrane. The outer portion of the space between the electrodes was gasketed by Viton sheets with the 5 cm^2 area over the electrodes cut out. Electrolytes were fed into the cell through fluorinated ethylene propylene tubing (inner diameter = 1/16') at a rate of 30 ml min^{-1} controlled by a KNF (IP50 10–26.4 V NFB 25 KTDCB-4B) diaphragm pump. The flow meter used in the gas outlet was the FMA-4305 from Omega, whereas the CO$_2$ sensor was the K33 ICB 30% from CO2Meter.

For all pH-swing and CO$_2$ capture experiments the excess-capacity electrolyte comprised 10 ml of 10 mM K$_3$Fe(CN)$_6$ and 10 mM of K$_4$Fe(CN)$_6$ dissolved in 1 M KCl. The other electrolyte comprised either 1 M KCl or artificial seawater, and its pH was measured continuously via a Mettler Toledo pH probe that was connected to a Hanna Instruments pH meter and a Biologic VSP-300 potentiostat. Artificial seawater was prepared by dissolving Instant Ocean Sea Salt in DI water; 0.36 g of the salt was dissolved in 10 ml of deionized water to achieve a specific gravity of 1.022.

For measurements of the intrinsic pH-swing characteristics of a given electrode, we sought to curtail the role of oxygen in contributing to pH swing. To remove electrode-absorbed oxygen, each electrode was placed in a vacuum chamber at a gauge pressure of −500 torr for 5 min before assembly in the flow cell. To remove dissolved oxygen in the electrolyte, the electrolytes were purged for 15 min and blanketed with pure nitrogen gas before and throughout each cycling experiment, respectively. A Biologic VSP-300 potentiostat was used for all cell cycling measurements.

Results

Electrochemical model of CO$_2$ separation driven by immobilized PCET agents.—We have constructed a 1-D continuum reaction-transport model that simulates pH-swing-driven CO$_2$ capture into and release from aqueous solution using immobilized PCET agents. The modeling domain (Fig. 1) consists of an aqueous electrolyte in contact with a planar film containing homogeneously distributed PCET-active moieties and a conducting substrate. The model accounts for the influence of several factors on the film's cycling behavior and the energetic cost of CO$_2$ concentration in the absence of oxygen, and thus the absence of side reactions between oxygen and the reduced form of the PCET-active molecule. These factors include: the applied current density, areal loading of PCET moieties in the film, series resistance of the cell, the rate constant for PCET (k$_{s,PCET}$), CO$_2$ reactivity with the electrolyte, and the diffusivity of protons within the PCET-active film (D$_H$).

The rate of 2H$^+$, 2e$^-$ PCET was assumed to be governed by Butler-Volmer kinetics, and to occur at the polymer|electrolyte interface, where reduction or oxidation of the PCET-active species is accompanied by proton transfer from the electrolyte into the film,
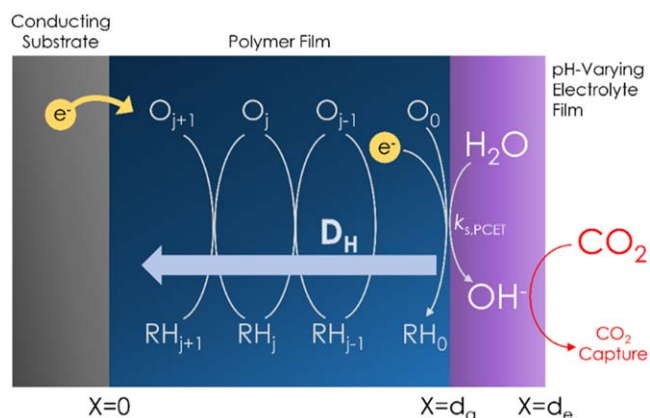

Figure 1. 1-D continuum reaction-transport model domain. PCET transforms O into RH at the polymer|electrolyte interface upon application of a reducing current and triggers CO$_2$ capture via a pH increase within the electrolyte. Homogeneous electron-coupled proton transport within the polymer film converts O to RH or vice versa. The polymer film and electrolyte have thicknesses of d$_a$ and d$_e$—d$_a$, respectively.

or vice versa, respectively. Electron-coupled proton transfer within the film was assumed to be governed by diffusion. We also assumed that dissolved CO$_2$ is in equilibrium with bicarbonate and carbonate species based on the two pK$_a$ values for carbonic acid. CO$_2$ capture at the electrolyte-gas boundary was rate-limited by liquid-phase CO$_2$ diffusion and either hydration (CO$_2$ + H$_2$O → HCO$_3^-$ + H$^+$) or hydroxylation (CO$_2$ + OH$^-$ → HCO$_3^-$), (see Eq. S10) whereas the rate of CO$_2$ release R$_{release}$ was governed by a physical desorption process,[37] such that:

$$-R_{release} = k_L([CO_{2,bulk}] - [CO_{2,gas}]) \qquad [1]$$

where [CO$_{2,bulk}$] is the CO$_2$ concentration in equilibrium with bulk electrolyte, [CO$_{2,gas}$] is the CO$_2$ concentration in equilibrium with the gas phase according to Henry's Law, and k$_L$ is the mass transfer coefficient of CO$_2$. More details about the model's assumptions and execution are provided in the Supplementary Information.

Figure 2 reports the voltage, DIC, pH, and state of charge (SOC) at the polymer film|electrolyte film interface as a function of time during a simulated pH swing cycle in which CO$_2$ is absorbed from a 410 ppm feed, concentrated, and released to 5% CO$_2$ (0.05 bar). SOC refers to the fraction of PCET-active species in the reduced form. The cycle was run at a current density of 1 mA cm^{-2} and included a 400 s rest period between the end of reduction and start of oxidation. The film's thickness and areal loading of PCET agents were 0.5 μm and 1 × 10^{-6} mol cm^{-2}, respectively, whereas D$_H$ was 10^{-8} cm^2/s. Other operational parameters are gathered in Table S1.

We assumed the presence of a stagnant aqueous electrolyte layer with a low thickness of 5 μm, so that the PCET capacity in the film would induce a large pH swing, and thus rapid CO$_2$ capture from the 410 ppm feed. Upon reduction, there is a clear increase in the SOC and pH of the film and electrolyte respectively, and both occur together with a steady increase in DIC as a result of CO$_2$ capture. The opposite processes are observed upon oxidation. The energetic cost of CO$_2$ concentration (W$_{CO_2}$) was calculated by taking the cyclic integral of potential with respect to charge passed, and dividing the result by net DIC released to the CO$_2$ collection stream:

$$W_{CO_2} = \frac{\oint jE \, dt}{\Delta DIC \times RF \times (d_e - d_a)}. \qquad [2]$$

Here, E is the cell potential, j is the current density, ΔDIC is the change in the total DIC concentration (i.e., the amount of CO$_2$ released) during oxidation, and RF is the roughness factor of the electrode. Applying this formula to the data in Fig. 2 yielded
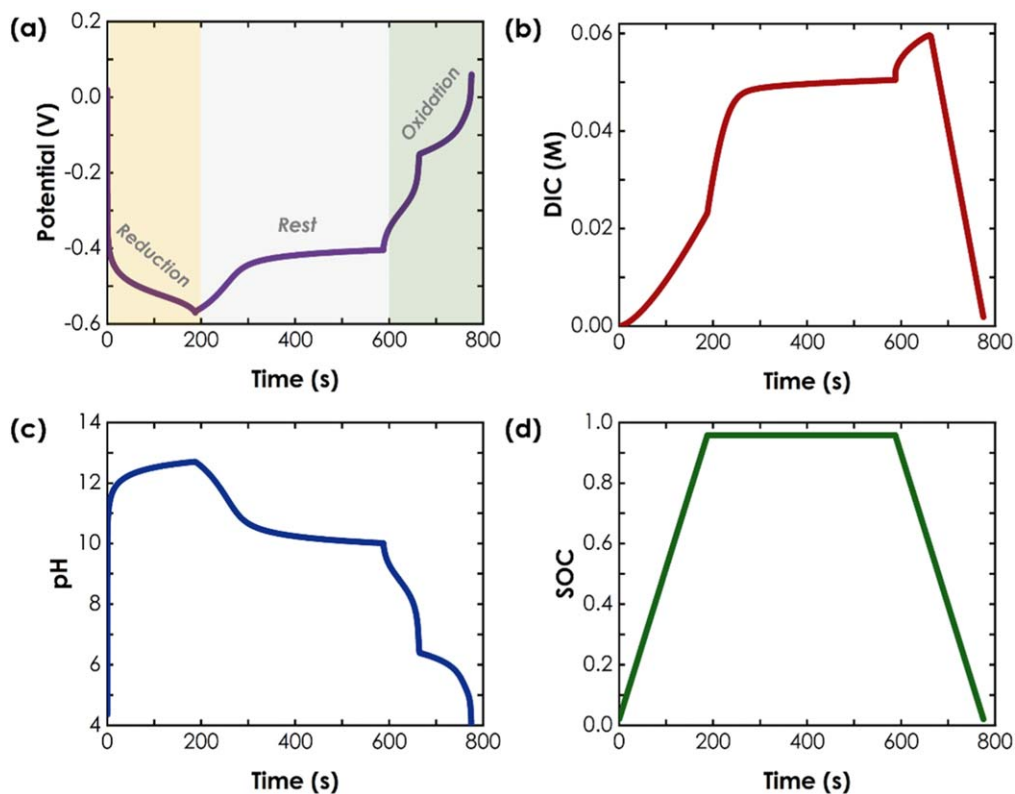
Figure 2. Simulation of a single CO_2-concentrating cycle at 1 mA cm^{-2} with CO_2 absorbed from a 410 ppm feed during the reduction half-cycle and rest period, and released to a 5% CO_2 exit stream during oxidation. Plots of (a) anode potential, (b) DIC in the electrolyte, (c) pH, and (d) SOC vs time. pH and DIC are taken from the polymer film|electrolyte interface. For each plot, reduction, rest, and oxidation occur between 0–200 s, 200–600 s, and 600–800 s, respectively, as annotated in (a).

125 kJ/mol$_{CO2}$. Figures S1–S4 show the dependence of this energetic cost of CO_2 concentration on j, RF, the areal loading of the PCET agents, and the exit stream's partial pressure, respectively. We also simulated a CO_2-concentrating cycle with a much larger, 0.1 cm-thick electrolyte (Fig. S5), in which a uniform solution composition (i.e., proton and DIC concentration) was enforced to mimic convective mixing of a bulk aqueous electrolyte in contact with the polymer film. The larger electrolyte volume with respect to the same PCET capacity lowers the upper pH limit that is achievable upon reduction, which in turn decreases the rate of CO_2 capture and thus the total increase in DIC from 50 mM (Fig. 2b) to 0.4 mM (Fig. S5b). Because of the lower ΔDIC, we reduced the exit stream's partial pressure by a factor of 10, from 0.05 to 0.005 bar, so that there would be a net decrease in DIC during the oxidation step. These conditions resulted in a 12.5-fold increase in the concentration of electrochemically pumped CO_2, from 400 ppm to 0.5%, at an energetic cost of 93 kJ/mol$_{CO2}$. Higher concentration factors are achievable with higher ratios of PCET agent loading to electrolyte volume. Nevertheless, these results indicate that electrode-bound PCET agents can drive CO_2 separation via reversible pH swings at reasonable energetic costs and motivate the fabrication of electrodes with immobilized and homogeneously distributed PCET-active moieties.

Vapor phase synthesis and characterization of Poly(1-aminoanthraquinone).—As noted earlier, vapor phase synthesis can conformally coat conjugated polymers over substrates with large roughness factors, making it an ideal technique for producing electrodes with high areal loadings over textiles. However, to the best of our knowledge, there are no examples of monomers that undergo PCET being polymerized using vapor phase synthesis. We note that anthraquinones are a suitable candidate for CO_2 capture using pH swing as they undergo PCET in solution and when immobilized or absorbed as monolayers,[38–41] yet C-C bond coupling is not observed between anthraquinones in the presence of a chemical oxidant, thereby limiting their amenability to oxidative polymerization from the vapor phase. We instead identified 1-aminoanthraquinone (1-AAQ) as a promising, commercially available alternative given the aniline moiety is susceptible to oxidation and subsequent C-C coupling.[42] Although 1-AAQ has a relatively large enthalpy of sublimation[43] compared with other monomers used for vapor phase synthesis,[36] we employed a custom-built, quartz hot-wall reactor with truncated path-lengths to easily intersect vapors of 1-AAQ with the oxidant iron (III) chloride (FeCl$_3$).

The chamber and deposition parameters used for the reaction are depicted in Fig. 3a along with chemical structures of 1-AAQ and its polymer (Fig. 3b). The deposited films appear purple following oxidation by FeCl$_3$, whereas 1-AAQ is a vibrant red color by comparison (Fig. S6). Given this is the first report of 1-AAQ being oxidatively coupled from the vapor phase, we isolated soluble fractions of the films for further analysis to confirm oligomerization or polymerization. The Ultraviolet-visible (UV–vis) absorption spectra of 1-AAQ and soluble fractions of PAAQ are shown in Fig. 3c. The spectrum of 1-AAQ exhibits a λ_{max} at 470 nm corresponding to its lowest-energy absorption band. In contrast, the absorption spectrum of dissolved PAAQ has a lowest-energy λ_{max} that is bathochromically shifted to 580 nm, indicating chemical species are present with longer conjugation lengths than 1-AAQ. The lowest-energy absorption maximum of a deposited thin film (613 nm) was red-shifted further than the soluble fractions of PAAQ in solution (Fig. S7), and the R_{rms} of the film was measured as 7.950 nm using atomic force microscopy (Fig. S8). These findings are consistent with others reported for poly(1-aminoanthraquinones) polymerized in solution.[42] We also measured the degree of polymerization of the soluble fractions of PAAQ using laser-desorption ionization mass spectrometry (LDI-MS) (Fig. 3d). Assuming a
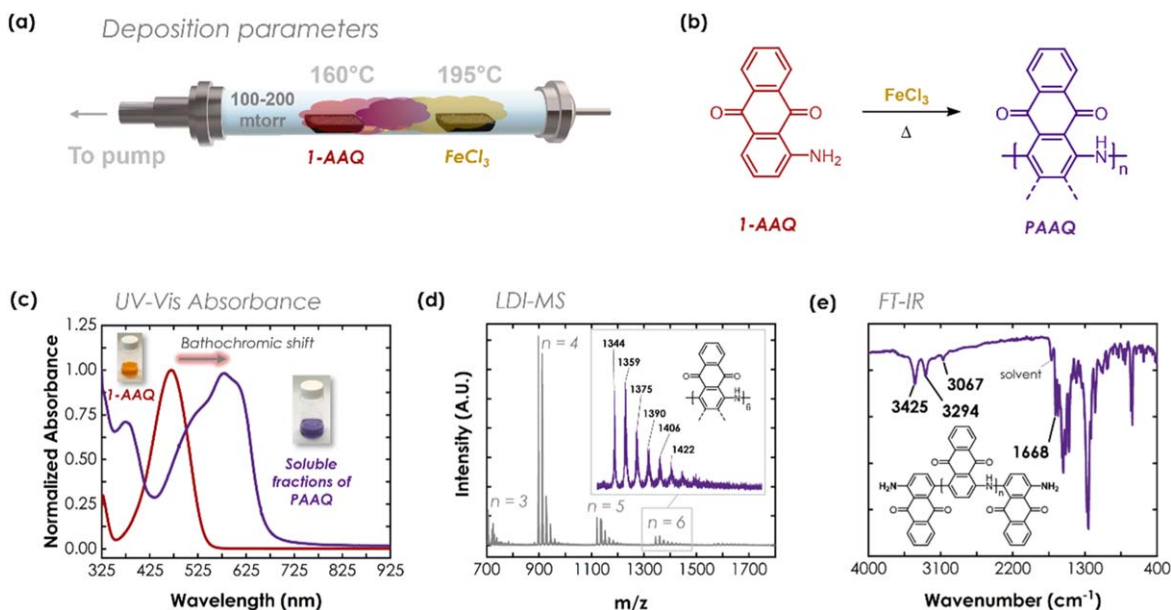
Figure 3. (a) Reactor schematic and parameters used to synthesize and deposit PAAQ. (b) Oxidative polymerization reaction between 1-AAQ and FeCl$_3$. (c) UV–vis absorbance spectra of 1-AAQ (red) and soluble fractions of PAAQ (purple) dissolved in acetone. Insets are images of representative samples. (d) LDI mass spectrum of PAAQ soluble fractions. (e) AT-IR spectrum of PAAQ soluble fractions.

repeat unit molecular weight of 221.21 g mol^{-1}, the mass spectrum indicates soluble fractions of PAAQ extend out to hexamers, consistent with our findings from UV–vis absorption measurements.

The concentration of soluble fractions extracted from the PAAQ films was insufficient to acquire an interpretable ^{1}H nuclear magnetic resonance spectrum. We instead used attenuated total reflectance infrared (AT-IR) spectroscopy to confirm if amine and quinone moieties were present in the soluble fractions of PAAQ. The AT-IR spectrum of these soluble fractions is shown in Fig. 3e and is comparable to that of 1-AAQ (Fig. S9). The PAAQ spectrum exhibits four notable bands outside the fingerprint region: (1) a carbonyl stretching band located at 1668 cm^{-1}, (2) an sp^2 C-H stretching band at 3067 cm^{-1}, and (3) two bands at 3294 cm^{-1} and 3425 cm^{-1} corresponding to the symmetric and asymmetric N-H stretching of primary amines. The third observation is expected given the soluble fractions are oligomeric and contain a large proportion of primary amines from end groups relative to secondary amines along the conjugated backbone.

We deposited PAAQ films onto graphite-felt substrates and used them as conductive working electrodes to measure cyclic voltammograms (CVs) (Fig. S10). The CV measurements indicate PAAQ undergoes quasi-reversible electrochemistry at pH 2.1, 4.2, 10, and 12, with their respective reduction potentials at 0.13, −0.04, −0.35, and –0.45 V vs Ag/AgCl. A linear fit of the Pourbaix diagram in Fig. S10c yields a slope of –57.7 mV pH^{-1}, corresponding to a 2H$^+$, 2e$^-$ transfer process. These results indicate anthraquinone moieties remain intact in our films, consistent with the AT-IR spectrum presented above, and can undergo PCET over a sufficient potential window for our purposes.

Electrode design and fabrication.—We attempted to incorporate graphite felt electrodes coated with PAAQ into redox flow cells for CO$_2$ capture using pH swing. Graphite felt electrodes were chosen given they are a standard material used in the flow battery literature.[44] Nonetheless, we found graphite felt induces an irreversible rise in pH from 4.5 to 10 in the pH-varying electrolyte of our flow cells. This behavior obscures our pH measurements and is likely caused by irreversible electrochemical reactions involving surface oxides.[45] The results and experimental parameters of these measurements are presented in Fig. S11. Suffice it to say, care must

be taken when selecting substrates for vapor deposition and CO$_2$ capture using pH swing.

To circumvent graphitic materials with surface-bound oxides, commercially available, blended wool felt (WFB) textiles were chosen as substrates over graphite felt following visual and tactile inspections to ensure their roughness factors and mechanical properties were comparable. Given WFB textiles are resistive, vapor phase synthesis was used to coat 5 cm^2 swatches with persistently *p*-doped PEDOT:Cl in general accordance with prior procedures.[46] Scanning electron microscopy (SEM) images of pristine and PEDOT-coated WFB fibers are presented in Figs. 4a and 4b, respectively. The images show PEDOT:Cl films conform uniformly over the cuticle cells of the fibers, allowing more material to be immobilized than would otherwise. Indeed, the resistance of the WFB swatches dropped considerably to 150 Ω/cm^2 following coating with PEDOT:Cl, and charging observed in SEM images was reduced substantially (Fig. S13). We incorporated these redox electrodes into our flow cells and measured the pH-varying electrolyte while oscillating the cell potential. The results are plotted in Fig. S12 and show that WFB textiles coated with PEDOT:Cl induce a sufficiently small, reversible pH change (ca. 1.5 units) in the pH-varying electrolyte upon cycling, likely stemming from PCET-active amino acid residues in wool. These findings contrast starkly with the irreversible pH changes induced by graphite felt electrodes and suggest WFB swatches coated with PEDOT:Cl are an ideal textile scaffold for our purposes.

Considering charge trapping and high resistivity are problems that plague 1-AAQ,[47] we fabricated electrodes with architectures that maximized contact between PAAQ and PEDOT:Cl (Fig. S14).[48] First, vapor phase synthesis was used to deposit PAAQ onto WFB blend textiles pre-coated with PEDOT:Cl. Finally, an additional layer of PEDOT:Cl was deposited over PAAQ to act as a conductive binder. Images of the electrode were acquired using SEM and are provided in Fig. S13. The deposited films uniformly coat the length and circumference of the WFB fibers and obscure any surface features, such as cuticle cells. Furthermore, void spaces are present along the surface of the coating that help increase surface area (Fig. 4d). Energy-dispersive X-ray spectroscopy (EDX) was used to map the distribution of atomic elements in blended films of PEDOT:Cl and PAAQ (Fig. 4e). EDX mapping shows sulfur, chlorine, and
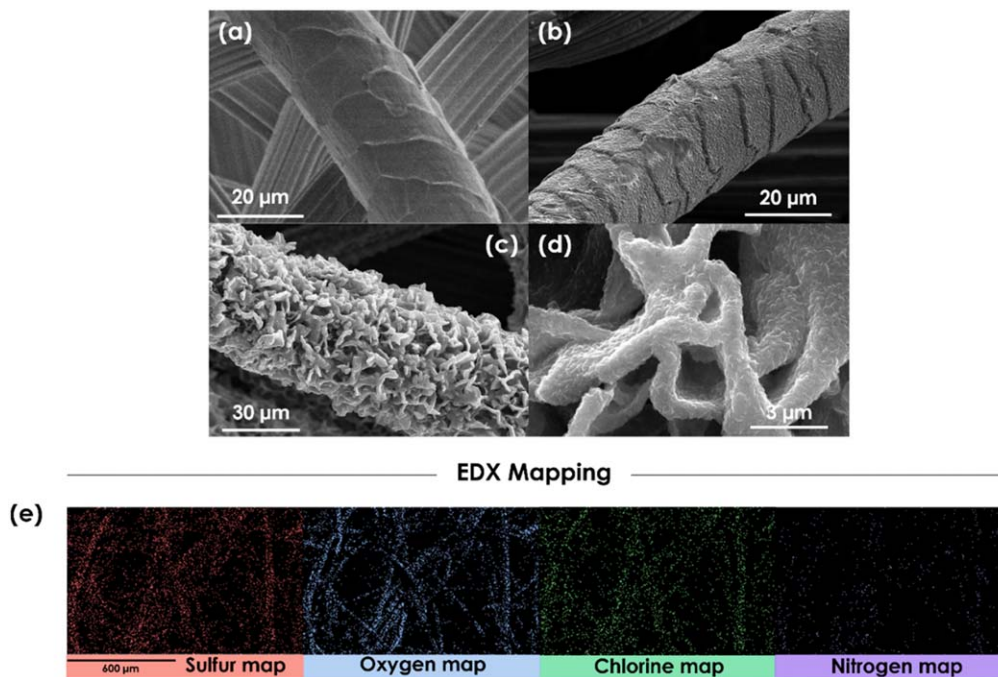
Figure 4. SEM images of (a) pristine wool felt blend fibers, (b) wool felt blend fibers coated with PEDOT:Cl, (c) and (d) wool felt blend fibers coated sequentially with PEDOT:Cl, PAAQ, and PEDOT:Cl. (e) EDX mapping of atomic elements in blended films of PEDOT:Cl and PAAQ coated over blended wool felt textiles.

oxygen are present in the films, all of which correspond to PEDOT:Cl and are uniformly distributed across the surface of the textile. Nitrogen atoms were also detected and evenly distributed, suggesting vapor phase synthesis can uniformly coat PAAQ across microtextured surfaces.

Carbon capture using pH swing.—We tested whether the PAAQ electrode could induce reversible pH swings in a bulk aqueous solution by integrating it into one side of a flow cell and circulating 10 ml of 1 M KCl through it while oscillating the cell potential. The electrode was separated from an excess-capacity ferrocyanide counter electrolyte by a cation-exchange membrane, and a pH probe immersed in the KCl solution provided continuous measurements of pH. Figure 5 presents a schematic of the experimental setup.

The initial pH of the KCl solution was adjusted to a value between 5 and 6 by adding aliquots of either diluted HCl or KOH solution. We performed galvanostatic cycling at 0.15 and 0.075 mA cm^{-2} while reducing and oxidizing the PAAQ electrode, respectively (Fig. 6); ideally, the former would lead to deacidification of the KCl solution, and the latter to acidification. The PAAQ reduction and oxidation half cycles ended with potential holds at 1.3 V and –0.4 V until the current density dropped to 0.075 mA cm^{-2} and 0.01 mA cm^{-2}, respectively. A switch from oxidation to reduction was also triggered once the pH-varying electrolyte reached pH 5. We expect that redox reactions are charge-balanced by passage of K$^+$ rather than Cl$^-$ ions across the cation-exchange membrane because for salt solutions of 1 M, Donnan potentials of up to ~ 30 mV have been measured, which will exclude co-ions.[49] The KCl solution was purged/blanketed with nitrogen gas
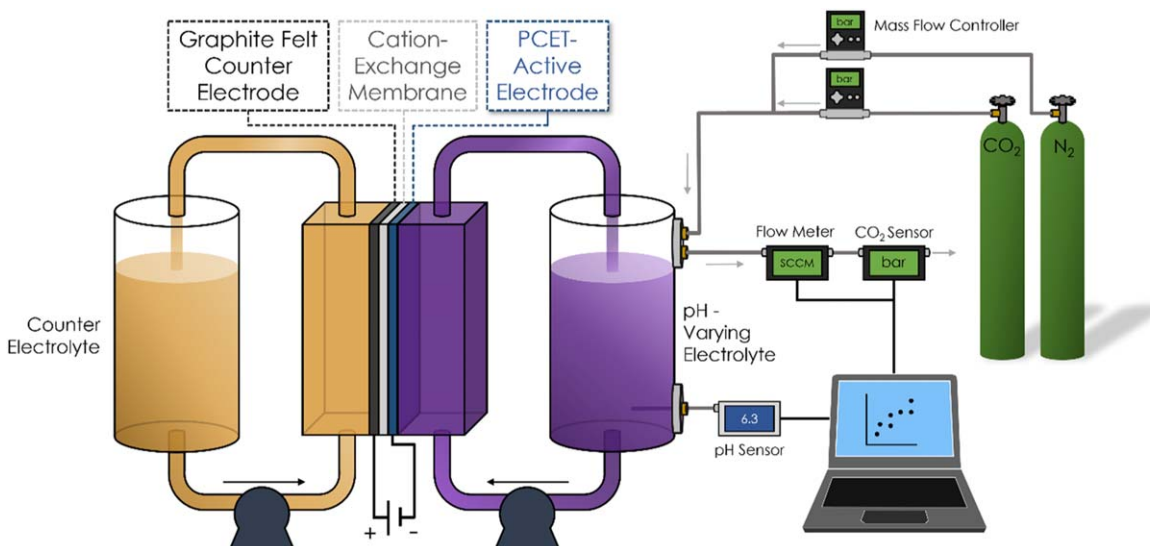

Figure 5. Schematic of the experimental setup used for measuring CO$_2$ capture and release from various feeds. The pH-varying electrolyte consists of an aqueous, 1 M KCl solution, unless otherwise stated, and the counter electrolyte is an aqueous solution of ferrocyanide prepared at excess-capacity.
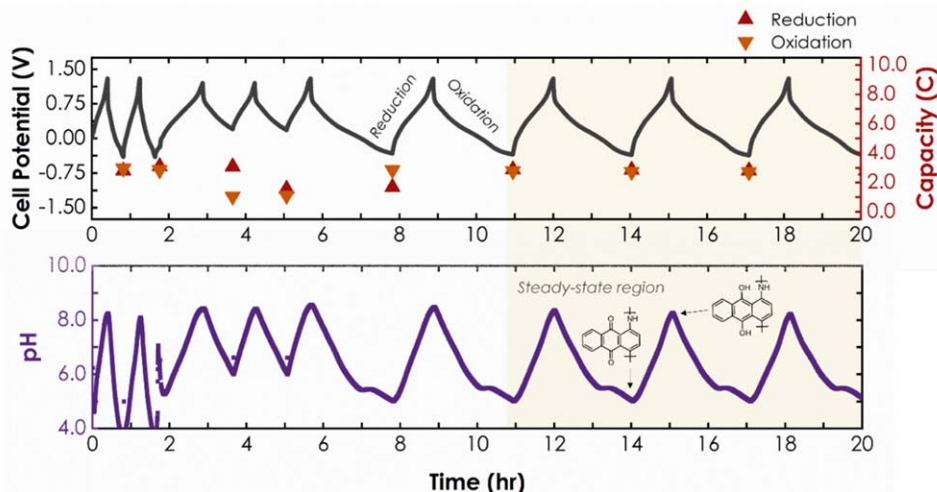
Figure 6. Experimental results from electrochemically cycling the PAAQ electrode in the absence of CO_2. Plots of the cell potential (top), capacity (top), and pH of the KCl solution (bottom) as a function of time are provided.

before and during these measurements to avoid oxygen reduction and to isolate the intrinsic pH-swing properties of the PAAQ electrode. The pH of the KCl solution increased from 5 to 8.3 during reduction of the PAAQ electrode—consistent with PCET-driven removal of protons from solution—and decreased back to 5 upon oxidation. This trend was steadily maintained for about 6 cycles, which lasted for a total of 18 h. At steady state, an electrode capacity of 2.8 C was accessed, at an average current efficiency of 97%. Given that less than 2.8 C of PCET capacity is theoretically required for the 3.3 pH unit swing, some of the capacity may be attributable to PEDOT, which is known to have capacitive properties.[50] Comparing measurements of the PAAQ electrode with the PEDOT:Cl control presented in Fig. S12 suggests PAAQ is necessary to induce a pH swing of 3.3 units, more than double what was induced by the control. Further studies are required for a more definitive assessment of the distribution between PEDOT and quinone capacity. Nevertheless, the steady capacity utilization and high current efficiency confirm that side reactions such as water splitting play a negligible role in pH swing, and that the PAAQ electrode could reliably drive CO_2 capture and release.

To explore this possibility, we cycled the PAAQ electrode while the KCl solution was in contact with a steady flow of premixed N_2/CO_2 gas with a CO_2 partial pressure of approximately 0.012 bar (12,000 ppm) (Fig. 7). The inlet gas flow rate was fixed by a mass flow controller to 2 ml min^{-1}, while the CO_2 partial pressure and total flow rate of the effluent gas were measured using a CO_2 sensor and digital flowmeter, respectively. Reduction of the electrode resulted in an increase in pH from 5 to an average of 6.4, and a simultaneous decrease in the partial pressure of CO_2 of the effluent gas below the 0.012 bar baseline, corresponding to CO_2 absorption into the electrolyte. Oxidation of the electrode returned the pH to 5 and caused a transient increase in the partial pressure above the CO_2 baseline, corresponding to CO_2 release. These concerted changes in pH and CO_2 partial pressure were repeated over 35 consecutive cycles, which took 100 h (about 4 d). Taking the CO_2 flow rate to be the product of CO_2 partial pressure and total flow rate, we estimated an average of 0.046 ml of CO_2 was stably absorbed and released per cycle. During PAAQ reduction, the increase in solution pH to 6.4 rather than 8.3 (as was observed for CO_2-free pH cycling) is rationalized by the pH buffering effect of CO_2 absorption. Indeed, the pH profile in the presence of CO_2 was reasonably well replicated by the reaction-transport model introduced above with a D_H of 10^{-8} cm^2/s, and assuming a polymer film thickness of 0.5 μm (see Fig. S15). We evaluated the average energetic cost of experimental CO_2 capture and release as 197 kJ/mol$_{CO_2}$ using Eq. 3:

$$W_{CO_2,exp} = \frac{\oint jAE\,dt}{\frac{P_{atm}V_{CO_2}}{RT}}. \qquad [3]$$

P_{atm} is atmospheric pressure, V_{CO_2} is the total volume of CO_2 released in one cycle, A is the geometric area of the electrode, R is the universal gas constant (8.314 J mol^{-1} K^{-1}) and T is temperature. V_{CO_2} is evaluated using Eq. 4:

$$V_{CO_2} = \int \dot{V}\frac{pCO_{2,corrected}}{100}dt \qquad [4]$$

where $\dot{V}$ is the total gas flow rate and $pCO_{2,corrected}$ is the baseline-corrected percentage of CO_2 in the total flow measured by the CO_2 sensor.

We then tested the chemical stability of the PAAQ electrode in the presence of oxygen by cycling the flow cell while the KCl solution was in continuous contact with air. Figure 8 presents results of 5 h of pH-swing cycling at 0.2 and 0.1 mA cm^{-2} during electrode reduction and oxidation, respectively. During the first deacidification half cycle, a plateau in the cell potential that was not present during oxygen-free cycling emerged at 0.42 V and is consistent with electrochemical oxygen reduction. Electrochemical reduction of PAAQ and oxygen would be expected to consume more protons than PAAQ reduction alone, and thus cause an irreversible increase in pH because the protons consumed in oxygen reduction are not released in the subsequent discharge half cycle. Accordingly, the pH of the KCl solution increased from ca. 5 to a higher terminal pH than was achieved for oxygen-free deacidification (9.2 vs 8.3) and fell upon acidification to 7, short of the initial value of 5. Manual addition of a small aliquot of HCl solution returned the pH to 5. We repeated this hybrid electrochemical-manual pH cycling protocol for 5 h, and found that the trends in pH, cell potential, and capacity were reproducible. The additional capacity originating from oxygen reduction manifested in a low average current efficiency, around 50%. Nevertheless, a consistent discharge capacity of about 1 C was accessed, which suggests that whereas *electrochemical* oxygen reduction occurs at the PAAQ electrode, the reduced quinone moieties on PAAQ are chemically stable in the presence of oxygen. In other words, immobilization of the quinone moieties on PAAQ confers resistance of their reduced form to chemical oxidation by oxygen, which enhances the practicality of CO_2 capture from air.

Encouraged by these results, we tested the PAAQ electrode's potential for CO_2 capture and release from and to an ambient air feed
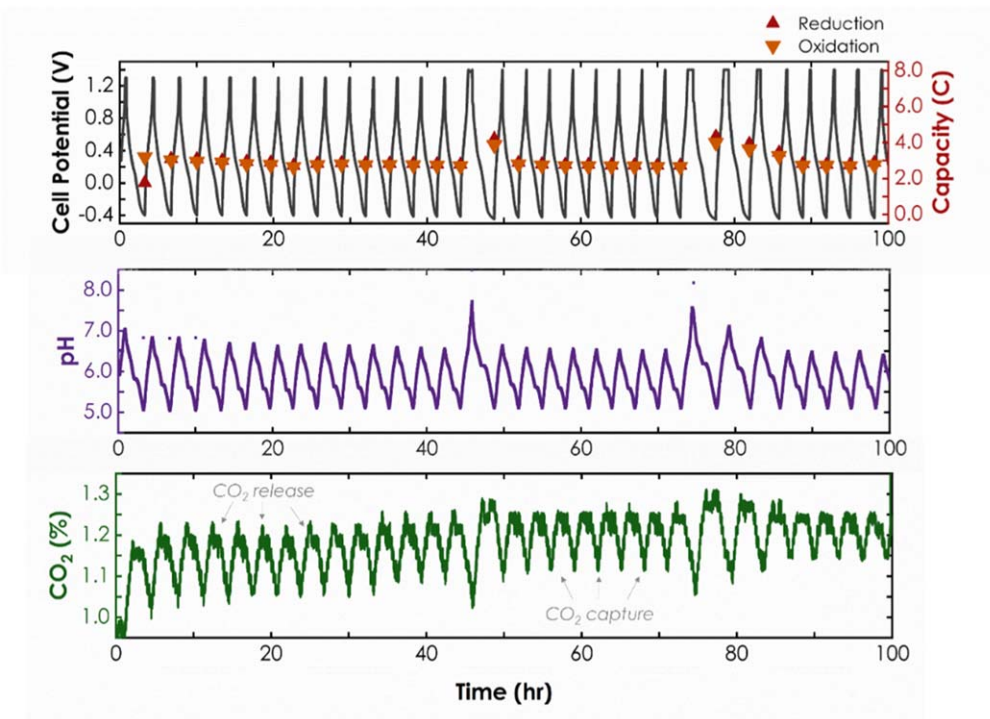
Figure 7. Experimental capture and release results from electrochemically cycling the PAAQ electrode in the presence of CO_2 at 0.012 bar. Plots of the cell potential (top), capacity (top), pH of the KCl solution (middle), and partial pressure of CO_2 in the cell's headspace (bottom) vs time are provided. The average baseline for the partial pressure of CO_2 was 1.17% over 100 h. The current density during reduction was 0.15 mA cm^{-2} and the current density during oxidation was 0.075 mA cm^{-2}.
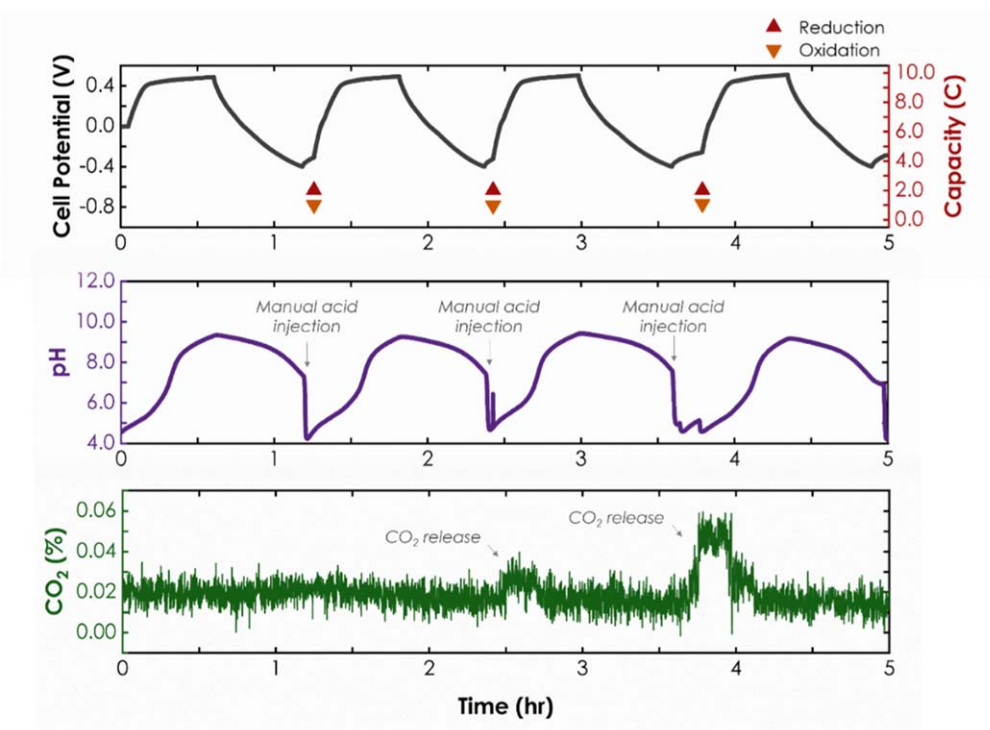

Figure 8. Experimental results from electrochemically cycling the PAAQ electrode in the presence of air. Plots showing the cell potential (top), capacity (top), pH of the KCl solution (middle), and partial pressure of CO_2 in the cells's headspace (bottom) vs time are provided.

(Fig. 9). Below pH 10, the [OH$^-$] is less than 0.1 mM, and CO_2 hydration rather than hydroxylation is expected to be the main mechanism for reactive CO_2 capture.[37] Because CO_2 has a low partial pressure in air, and CO_2 hydration has a low first-order rate

constant of 0.02 s^{-1},[37] we rested the cell for 4 h at open circuit after each PAAQ reduction half-cycle to prolong contact between the alkalized KCl solution and air, and thereby maximize CO_2 uptake. The reduction capacity was limited to 1.35 C to mitigate
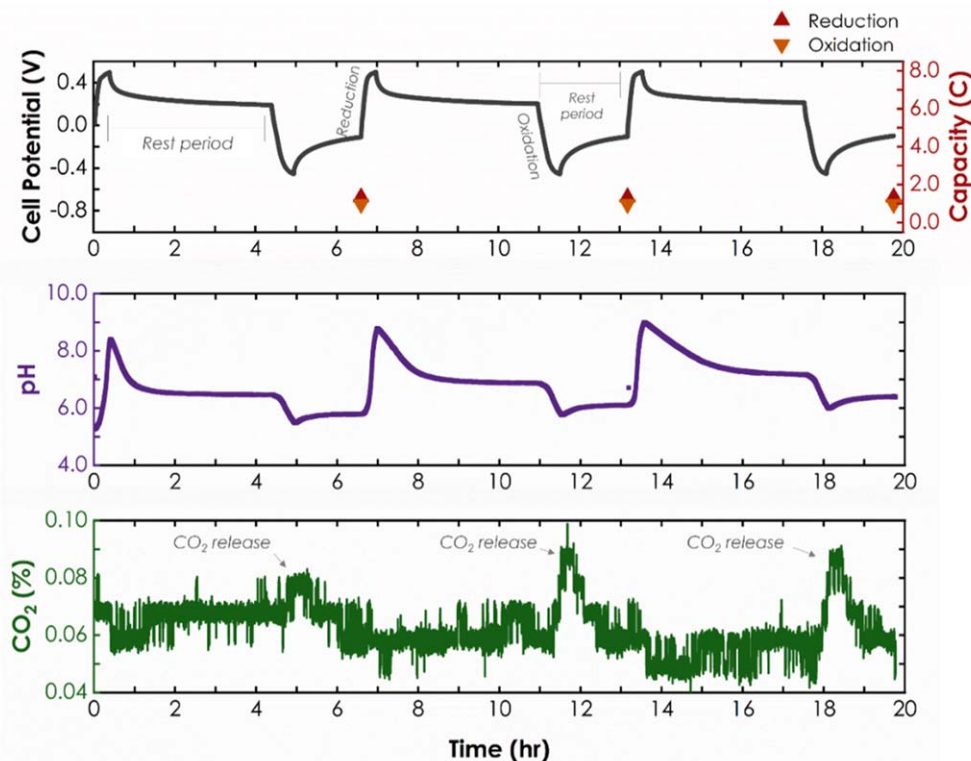
Figure 9. Experimental results from electrochemically cycling the PAAQ electrode in the presence of air with a 4 h rest period between cycles. Plots showing the cell potential (top), capacity (top), pH of the KCl solution (middle) and partial pressure of CO_2 in the cell's headspace (bottom) vs time are provided.

electrochemical oxygen reduction and irreversible proton consumption, which allowed the pH to drop low enough upon electrode oxidation for CO_2 release. Under these conditions, oxidation of the electrode decreased the pH from 7 (its steady-state value during the rest period) to 5.5 and caused a transient increase in the CO_2 partial pressure of the effluent gas flow, from a baseline of 600 ppm to a peak of ca. 900 ppm; this trend repeated over the last two consecutive cycles. The energetic cost of CO_2 separation based on Eq. 2 was 553 kJ/mol$_{CO2}$. This value is high but is attributable to the small amount of CO_2 absorbed from ambient air (0.015 ml/cycle).

Despite the 4 h rest in the presence of air, a constant oxidation capacity of 1 C was again accessed during the three acidification half cycles performed, corresponding to a current efficiency of 76%. This result again underscores the higher stability of reduced quinone moieties in the PAAQ electrode against chemical oxidation by oxygen relative to dissolved counterparts. To highlight this point further, we assembled a flow cell containing 10 mM of anthraquinone-2,6-disulfonic acid dissolved in an 0.1 M KCl solution and conducted a similar reduction-rest-oxidation cycling test in the presence of ambient air (Fig. S16). After the 3 h rest period, an oxidation capacity of ≈ 0 C was obtained, clearly because of oxidation of the reduced quinone species by oxygen in air.

The limited working pH range of the PAAQ electrode in the absence of CO_2 (5–8.3) gave rise to an impractically high energetic cost for direct air capture of CO_2. We realized, however, that this pH range is ideal for the recovery of CO_2 from seawater, which has an average pH of 8.2, and in which DIC is present predominantly as bicarbonate. Based on the known equilibrium between bicarbonate and CO_2 (effective pK_a = 6.1), a 3-unit pH decrease would be sufficient to convert most of the bicarbonate to neutral CO_2, which could then be removed and converted/sequestered. Because CO_2 is volumetrically more concentrated in seawater (100 mg l^{-1}) than atmosphere (0.77 mg l^{-1}), CO_2 removal from seawater is increasingly being recognized as an attractive route toward negative emissions.[6,51] Electrochemical pH-swing-based DIC removal from seawater has been recently demonstrated by Kim et al. in a

continuous-flow configuration using Ag and Bi electrodes in tandem flow cells.[52] We implemented a similar concept, but cycled the PAAQ electrode against artificial seawater (Fig. 10) in one flow cell, i.e., a batch-mode configuration. The KCl electrolyte was replaced after the second de-acidification half cycle with artificial seawater. During the subsequent acidification step, the pH of the seawater decreased from 8.2 to 6.3, which triggered CO_2 release, registered as a transient rise in the partial pressure of CO_2 in the effluent N_2 gas. 54% of the seawater DIC was removed at an energetic cost of 202 kJ/mol$_{CO2}$. This figure is higher than the 120 kJ/mol$_{CO2}$ achieved by Kim et al. and is comparable to values reported in other studies of electrochemical recovery of CO_2 from seawater based on hydrogen looping and bipolar membrane electrodialysis (BPMED), which range between 120[53] and 250 kJ/mol$_{CO2}$[7] at their low ends, respectively. Nevertheless, it is likely that our system will have a lower capital cost given it is constructed from abundant raw materials rather than rare elements, such as Ag and Pt.

Conclusions

We have used vapor phase synthesis to fabricate redox-active electrodes that comprise an immobilized PCET agent, PAAQ, and PEDOT:Cl as a charge collector, all conformally coated atop swatches of commercially available, blended wool felt textiles. The electrodes can be incorporated into redox flow cells to induce reversible pH swings in an aqueous electrolyte upon electrochemical cycling. As shown, this system facilitates pH-swing-driven carbon capture from gaseous sources (a 1% CO_2 feed and air), as well as seawater, with the latter at a competitively low energetic cost of 202 kJ/mol$_{CO2}$. The design differs from other carbon capture systems that use dissolved PCET agents by confining proton-storage to the surface of an electrode kept separate from an aqueous, CO_2-capturing phase, allowing both components to be optimized individually. Further, quinone moieties embedded within the electrode are more stable in the presence of oxygen, during reduction half-cycles, than dissolved counterparts, presumably due to inhibited
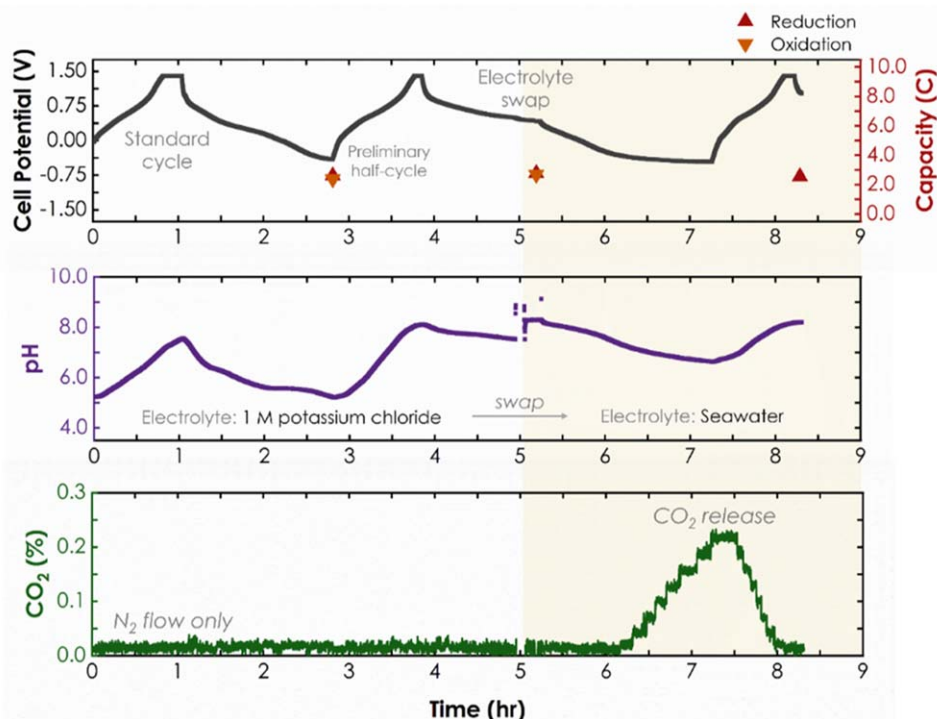
Figure 10. Experimental results from electrochemically cycling the PAAQ electrode in the presence of seawater. Plots of the cell potential (top), capacity (top), pH of KCl solution or seawater (middle), and CO_2 partial pressure of the cell's headspace (bottom) vs time are provided.

mass transport of O_2. The remarkable stability of these electrodes is useful for practical situations where oxygen is mixed with CO_2 in a feed of interest (e.g., air or flue gas).

The electrode in this study has a narrow pH range (5–8.5) that results in a low rate and high energetic cost (553 kJ/mol$_{CO2}$) of CO_2 capture from air. Nevertheless, simulations from a 1D reaction-transport model indicate lower energetic costs (<130 kJ/mol$_{CO2}$) should be possible if high loadings of polymer-bound PCET moieties (>10^{-6} mol cm^{-2}) with high pK_a values (>13) in their reduced forms are obtained (Fig. S3). Therefore, efforts to fabricate optimized electrodes should focus on increasing polymerization kinetics. For example, synthesizing volatile monomers with moieties that undergo PCET and oxidative polymerization, but that are electronically decoupled to maximize the highest occupied molecular orbital density at the latter. Further, the corresponding conjugated polymer should have a persistently doped backbone over a wide potential window to minimize resistivity throughout the electrode. Substituted phenazines, such as diaminophenazine, are an encouraging starting point as they are commercially available and the phenazine core possesses PCET-active groups with pK_a values of at least 13 in their reduced form.[54] Assembling a microfluidic electrochemical cell may be possible as well, such that the ratio of the PCET agent loading to the aqueous phase volume would be large enough to enable a very high local pH upon deacidification, and thus rapid capture and concentration of CO_2 from air (>0.04 mol m^{-2} h^{-1}) (Fig. S1). Because the active materials used in these electrodes comprise abundant elements, we envision, with further optimization, the possibility for widespread deployment of these electrochemical carbon capture systems at low commercial cost of separated CO_2.

ORCID

Trisha L. Andrew https://orcid.org/0000-0002-8193-2912
David G. Kwabi https://orcid.org/0000-0003-3663-8789

References

1. *Climate Change 2014: Synthesis Report*Rajendra Pachauri and Leo Meyer (ed.), (IPCC, Geneva, Switzerland) (2014).
2. V. Masson-Delmotte et al. (ed.), *An IPCC Special Report on the impacts of global warming of 1.5 °C Above Pre-Industrial Levels and Related Global Greenhouse Gas Emission Pathways, in the Context of Strengthening the Global Response to the Threat of Climate Change, sustainable development, and efforts to eradicate poverty* (IPCC, Cambridge, UK and New York, NY, USA) (2018).
3. B. Metz, O. Davidson, H. de Coninck, M. Loos, and L. Meyer (ed.), *IPCC Special Report on Carbon Dioxide Capture and Storage* (IPCC, Cambridge University Press, Cambridge, United Kingdom and New York, NY) (2005).
4. M. Zhang, W. Wei, S. Zhou, D.-D. Ma, A. Cao, X.-T. Wu, and Q.-L. Zhu, "Engineering a conductive network of atomically thin bismuthene with rich defects enables CO2 reduction to formate with industry-compatible current densities and stability." *Energy Environ. Sci.*, **14**, 4998 (2021).
5. D. W. Keith, G. Holmes, D. St. Angelo, and K. Heidel, "A process for capturing CO2 from the atmosphere." *Joule*, **2**, 1 (2018).
6. *A Research Strategy for Ocean-based Carbon Dioxide Removal and Sequestration* (National Academies of Sciences, Engineering, and Medicine., Washington, DC) (2022).
7. R. Sharifian, M. Wagterveld, I. A. Digdaya, C. Xiang, and D. A. Vermaas, "Electrochemical carbon dioxide capture to close the carbon cycle." *Energy and Environmental Science*, **14**, 781 (2021).
8. M. Fasihi, O. Efimova, and C. Breyer, "Techno-economic assessment of CO2 direct air capture plants." *J. Clean. Prod.*, **224**, 957 (2019).
9. S. E. Renfrew, D. E. Starr, and P. Strasser, "Electrochemical approaches toward CO2 capture and concentration." *ACS Catal.*, **10**, 13058 (2020).
10. J. H. Rheinhardt, P. Singh, P. Tarakeshwar, and D. A. Buttry, "Electrochemical capture and release of carbon dioxide." *ACS Energy Lett.*, **2**, 454 (2017).
11. A. M. Zito et al., "Electrochemical carbon dioxide capture and concentration." *Chem. Rev.*, **123**, 8069 (2023).
12. B. Gurkan, F. Simeon, and T. A. Hatton, "Quinone reduction in ionic liquids for electrochemical CO2 separation." *Sustainable Chemistry and Engineering*, **3**, 1394 (2015).

13. H. Seo, M. Rahimi, and T. A. Hatton, "Electrochemical carbon dioxide capture and release with a redox-active amine." *Journal of the American Chemical Society*, **144**, 2164 (2022).

14. Y. Liu, H.-Z. Ye, K. M. Diederichsen, T. Van Voorhis, and T. A. Hatton, "Electrochemically mediated carbon dioxide separation with quinone chemistry in salt-concentrated aqueous media." *Nat. Commun.*, **11**, 2278 (2020).

15. M. B. Mizen and M. S. Wrighton, "Reductive addition of CO2 TO 9,10-Phenanthrenequinone." *J. Electrochem. Soc.*, **136**, 941 (1989).

16. P. Scovazzo, J. Poshusta, D. DuBois, C. Koval, and R. Noble, "Electrochemical separation and concentration of <1% carbon dioxide from nitrogen." *J. Electrochem. Soc.*, **150**, D91 (2003).

17. D. H. Apaydin, E. D. Glowacki, E. Portenkirchner, and N. S. Sariciftci, "Direct electrochemical capture and release of carbon dioxide using an industrial organic pigment: quinacridone." *Angewandte Chemie-International Edition*, **53**, 6819 (2014).

18. R. Tyburski, T. Liu, S. D. Glover, and L. Hammarström, "Proton-coupled electron transfer guidelines, fair and square." *Journal of the American Chemical Society*, **143**, 560 (2021).

19. M. Quan, D. Sanchez, M. F. Wasylkiw, and D. K. Smith, "Voltammetry of quinones in unbuffered aqueous solution: reassessing the roles of proton transfer and hydrogen bonding in the aqueous electrochemistry of quinones." *Journal of American Chemical Society*, **129**, 12847 (2007).

20. S. Jin, M. Wu, R. G. Gordon, M. J. Aziz, and D. G. Kwabi, "pH swing cycle for CO_2 capture electrochemically driven through proton-coupled electron transfer." *Energy and Environmental Science.*, **13**, 3706 (2020).

21. J. D. Watkins, N. S. Siefert, X. Zhou, C. R. Myers, J. R. Kitchin, D. P. Hopkinson, and H. B. Nulwala, "Redox-mediated separation of carbon dioxide from flue gas." *Energy & Fuels*, **29**, 7508 (2015).

22. C. Huang, C. Liu, K. Wu, H. Yue, S. Tang, H. Lu, and B. Liang, "CO2 capture from flue gas using an electrochemically reversible hydroquinone/quinone solution." *Energy & Fuels*, **33**, 3380 (2019).

23. H. Xie, Y. Wu, T. Liu, F. Wang, B. Chen, and B. Liang, "Low-energy-consumption electrochemical CO2 capture driven by biomimetic phenazine derivatives redox medium." *Appl. Energy*, **259**, 114119 (2019).

24. P. S. Guin, S. Das, and P. C. Mandal, "Electrochemical reduction of quinones in different media: a review." *International Journal of Electrochemistry*, **2011**, 1 (2011).

25. H. Seo and T. A. Hatton, "Electrochemical direct air capture of CO2 using neutral red as reversible redox-active material." *Nat. Commun.*, **14**, 313 (2023).

26. S. Jin, M. Wu, Y. Jing, R. G. Gordon, and M. J. Aziz, "Low energy carbon capture via electrochemically induced pH swing with electrochemical rebalancing." *Nat. Commun.*, **13**, 2140 (2022).

27. A. Hemmatifar, J. S. Kang, N. Ozbek, K.-J. Tan, and T. A. Hatton, "Electrochemically mediated direct CO2 capture by a stackable bipolar cell." *ChemSusChem*, **15**, e202102533 (2022), (acccessed 2023/04/24).

28. T. Winter, M. Bitsch, F. Müller, S. Voskian, T. A. Hatton, K. Jacobs, V. Presser, and M. Gallei, "Redox-responsive 2-Aminoanthraquinone core–shell particles for structural colors and carbon capture." *ACS Applied Polymer Materials*, **3**, 4651 (2021).

29. D. Bilger, S. Z. Homayounfar, and T. L. Andrew, "A critical review of reactive vapor deposition for conjugated polymer synthesis." *J. Mater. Chem. C*, **7**, 7159 (2019).

30. M. Heydari Gharahcheshmeh and K. K. Gleason, "Device fabrication based on oxidative chemical vapor deposition (oCVD) synthesis of conducting polymers and related conjugated organic materials." *Adv. Mater. Interfaces*, **6**, 1801564 (2019), (acccessed 2023/04/24).

31. L. Allison, S. Hoxie, and T. L. Andrew, "Towards seamlessly-integrated textile electronics: methods to coat fabrics and fibers with conducting polymers for electronic applications." *Chem. Commun.*, **53**, 7182 (2017).

32. S. E. Atanasov, M. D. Losego, B. Gong, E. Sachet, J.-P. Maria, P. S. Williams, and G. N. Parsons, "Highly conductive and conformal poly(3,4-ethylenedioxythiophene) (PEDOT) thin films via oxidative molecular layer deposition." *Chem. Mater.*, **26**, 3471 (2014).

33. H. Chelawat, S. Vaddiraju, and K. Gleason, "Conformal, conducting poly(3,4-ethylenedioxythiophene) thin films deposited using bromine as the oxidant in a completely dry oxidative chemical vapor deposition process." *Chem. Mater.*, **22**, 2864 (2010).

34. W. Viola, L. Zhang, and T. L. Andrew, "Oxidant aggregate-induced porosity in vapour-deposited polymer films and correlated impact on electrochemical properties." *Supramol. Chem.*, **31**, 491 (2019).

35. K. K. Gleason, "Nanoscale control by chemically vapour-deposited polymers." *Nature Reviews Physics*, **2**, 347 (2020).

36. D. Bilger, K.-W. Park, and T. L. Andrew, "A vapor printed electron-accepting conjugated polymer for textile optoelectronics." *Synth. Met.*, **250**, 1 (2019).

37. P. V. Danckwerts, *Gas-Liquid Reactions* (McGraw-Hill Book Co, New York, NY) (1970).

38. C. M. Hanna, A. Luu, and J. Y. Yang, "Proton-coupled electron transfer at anthraquinone modified indium tin oxide electrodes." *ACS Appl. Energy Mater.*, **2**, 59 (2019).

39. R. J. Forster and J. P. O'Kelly, "Protonation reactions of anthraquinone-2,7-disulphonic acid in solution and within monolayers." *J. Electroanal. Chem.*, **498**, 127 (2001).

40. G. C. Sedenho, D. De Porcellinis, Y. Jing, E. Kerr, L. M. Mejia-Mendoza, Á. Vazquez-Mayagoitia, A. Aspuru-Guzik, R. G. Gordon, F. N. Crespilho, and M. J. Aziz, "Effect of molecular structure of quinones and carbon electrode surfaces on the interfacial electron transfer process." *ACS Appl. Energy Mater.*, **3**, 1933 (2020).

41. F. V. Owhoso, S. V. Modak, P. Saha, and D. G. Kwabi, "Effect of covalent modification on proton-coupled electron transfer at quinone-functionalized carbon electrodes." *The Journal of Physical Chemistry C*, **127**, 3165 (2023).

42. X.-G. Li, H. Li, M.-R. Huang, and M. G. Moloney, "Synthesis and multi-functionality of self-stabilized poly(aminoanthraquinone) nanofibrils." *The Journal of Physical Chemistry C*, **115**, 9486 (2011).

43. K. Nishida, E. Ishihara, T. Osaka, and M. Koukitu, "Vapour pressures and heats of sublimation of some disperse dyes." *J. Soc. Dyers Colour.*, **93**, 52 (1977), (acccessed 2023/04/24).

44. K. M. Tenny, A. Forner-Cuenca, Y.-M. Chiang, and F. R. Brushett, "Comparing physical and electrochemical properties of different weave patterns for carbon cloth electrodes in redox flow batteries." *Journal of Electrochemical Energy Conversion and Storage*, **17**, 1 (2020), (acccessed 8/18/2020).

45. R. L. McCreery, "Advanced carbon electrode materials for molecular electro-chemistry." *Chem. Rev.*, **108**, 2646 (2008).

46. L. K. Allison and T. L. Andrew, "A wearable all-fabric thermoelectric generator." *Adv. Mater. Technol.*, **4**, 1800615 (2019), (acccessed 2023/04/24).

47. Z. Algharaibeh and P. G. Pickup, "Charge trapping in poly(1-amino-anthraquinone) films." *Electrochim. Acta*, **93**, 87 (2013).

48. S. Admassie, A. Elfwing, and O. Inganäs, "Electrochemical synthesis and characterization of interpenetrating networks of conducting polymers for enhanced charge storage." *Adv. Mater. Interfaces*, **3**, 1500533 (2016), (acccessed 2023/04/24).

49. P. Aydogan Gokturk, R. Sujanani, J. Qian, Y. Wang, L. E. Katz, B. D. Freeman, and E. J. Crumlin, "The Donnan potential revealed." *Nat. Commun.*, **13**, 5880 (2022).

50. L. Zhang and T. L. Andrew, "Using the surface features of plant matter to create all-polymer pseudocapacitors with high areal capacitance." *ACS Appl. Mater. Interfaces*, **10**, 38574 (2018).

51. E. C. La Plante, D. A. Simonetti, J. Wang, A. Al-Turki, X. Chen, D. Jassby, and G. N. Sant, "Saline water-based mineralization pathway for gigatonne-scale CO2 management." *ACS Sustainable Chemistry & Engineering*, **9**, 1073 (2021).

52. S. Kim, M. Nitzsche, S. B. Rufer, J. R. Lake, K. K. Varanasi, and T. A. Hatton, "Asymmetric chloride-mediated electrochemical process for CO2 removal from oceanwater." *Energy Environ. Sci.*, **16**, 2030 (2023).

53. L. Yan, J. Bao, Y. Shao, and W. Wang, "An electrochemical hydrogen-looping system for low-cost CO2 capture from seawater." *ACS Energy Lett.*, **7**, 1947 (2022).

54. R. C. Kaye and H. I. Stonehill, "The polarographic reduction of pyridine, quinoline, and phenazine." *Journal of the Chemical Society (Resumed)*, **619**, 3240 (1952).